Desalination 443 (2018) 198–211

Contents lists available at ScienceDirect

Desalination

journal homepage: www.elsevier.com/locate/desal

Cost-optimal design of a batch electrodialysis system for domestic desalination of brackish groundwater

Sahil R. Shah[a,*], Natasha C. Wright[a], Patrick A. Nepsky[b], Amos G. Winter V[a]

[a] Department of Mechanical Engineering, Massachusetts Institute of Technology, Cambridge MA, USA
[b] MIT Lincoln Laboratory, Lexington MA, USA

GRAPHICAL ABSTRACT

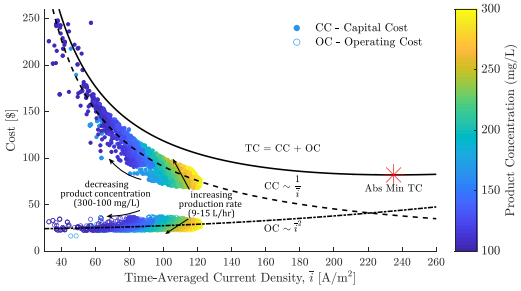

ARTICLE INFO

Keywords:
Electrodialysis
Optimization
Brackish
Point-of-use
Cost

ABSTRACT

This study presents the pareto-optimal design of a domestic point-of-use batch electrodialysis (ED) system. Specifically, the optimal geometry, flow-rates, and applied voltage for total cost minimization were explored for varying production rate (9–15 L/h) and product concentration (100–300 mg/L) requirements, while feed concentration and recovery ratio were maintained at 2000 mg/L and 90%, respectively. Capital cost dominated over energetic cost; hence, optimal designs maximized current density. Capital cost was significantly higher for 100 mg/L systems, than 200 and 300 mg/L: $141 vs. $93 and $79, at 12 ± 0.5 L/h of production. Pumps were an important consideration, contributing up to 46% of the total cost. Large membrane length-to-width aspect ratios (3.5:1 to 6:1) and thin channels (0.30–0.33 mm) promoted high current densities, and 11–21 cm/s velocities optimized mass transfer against pressure drop. Optimal voltages were 0.9–1.3 V/cell-pair at 9 L/h, and decreased at higher rates. Lastly, higher production was obtained primarily by increasing cell-pair area rather than number of cell-pairs (36–46). It was additionally observed that active area increased linearly with feed concentration (1500–2500 mg/L), while recovery (60–90%) minimally affected design. This work also suggests that voltage control during the batch process, and less expensive pumps, can further reduce cost.

1. Introduction

Domestic reverse osmosis (RO) systems are widely used in Indian homes to desalinate groundwater to a total dissolved salt (TDS) content that is suitable for drinking (less than 500 mg/L [1]), but they recover only 25–40% [2] of the feed. The domestic scale addressed here refers to point-of-use (POU) systems that typically produce 8–15 L/h of drinking water, store 7–10 L, weigh 8–11 kg, and are usually wall-mounted or placed on kitchen counters in individual homes [3,4]. Since the market for POU RO devices at this scale is forecast to grow at a compound annual growth rate of 18.2% between 2016 and 2024 [5], there is also a commercial incentive for developing more efficient

* Corresponding author.
E-mail address: sahils@mit.edu (S.R. Shah).

https://doi.org/10.1016/j.desal.2018.05.010
Received 1 December 2017; Received in revised form 3 April 2018; Accepted 16 May 2018
Available online 15 June 2018
0011-9164/

desalination solutions that operate at the same scale.

Given that the concentration of the groundwater underlying a majority of India is under 2000 mg/L, electrodialysis (ED) can provide a higher recovery and more energy-efficient desalination compared to RO for this domestic application [6,7]. Similarly, growing concern over water scarcity and the need for more energy-efficient desalination has also recently revived an interest in the possibility of using ED for brackish water desalination and tap-water softening in European cities [8].

Despite the interest surrounding the use of ED for domestic purposes, little work has been performed to characterize the design of an appropriate ED system for the application. Pilat developed and piloted more than 200 domestic ED units before 2001, but little information regarding cost or the design of the system was provided [9]. More recently, Thampy et al. investigated a hybrid approach whereby ED was used to initially desalinate 2000–4000 mg/L water to 500 mg/L and further desalination to 120 mg/L or lower thereafter was achieved using RO [10]. Given that their small-scale system operated in a continuous process, without the recirculation of product water, only 50–60% of the feed supply was recovered. Instead, Nayar et al. showed that it was feasible to implement ED solely in a batch architecture (Fig. 1), where product water is recirculated, to desalinate from 3000 mg/L to 350 mg/L, at a competitive production rate of 12 L/h while providing 80% recovery [11]. However, their system was not designed to minimize capital cost which was an estimated $206 for the entire system, $138 of which was attributed to the ED stack and pumps.

While Nayar et al. have demonstrated that batch ED is a viable technology for satisfying household desalination needs, further cost reduction is required to be competitive with existing RO devices which are priced between $200–$300. Therefore, in this work we investigated the pareto-optimal design of the proposed domestic batch ED system considering production rate, product water concentration, and cost using simulation. In particular, we aimed to address the following:

1. How should a domestic ED system be designed to minimize cost?
2. How do water quality and production requirements affect the design?
3. What are the primary contributors to cost?
4. What developments are necessary for further cost reduction?

Prior design and optimization work has been performed for large-scale systems which are typically operated in a continuous architecture [12] for industrial applications. For these systems, the pump cost and energy consumption are often neglected because they are low relative to cost of the ED stack and the energy consumed by desalination [13,14]. Optimization at the domestic scale presents a different scenario where the pumps were found to strongly affect the cost, energy consumption, and performance of the ED system.

In addition, minimization of operating costs is often the most important consideration in industrial applications whereby the energy consumption can not be neglected [15]. In the present study, it was found that capital cost was the dominant factor affecting the affordability of the domestic system.

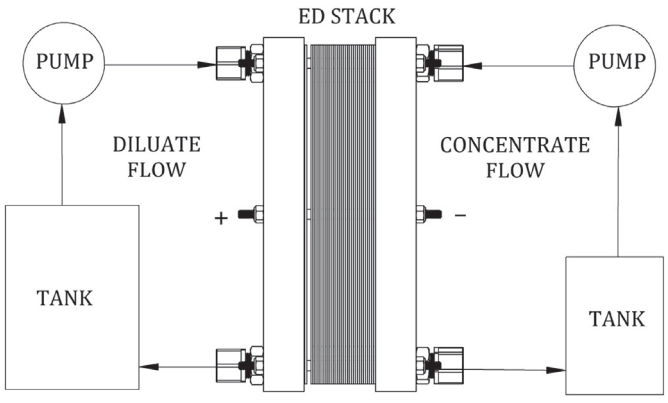

Fig. 1. Schematic of proposed domestic ED system operating in batch mode.

2. System description

The batch ED system (Fig. 1) proposed by Nayar et al. [11] and analyzed here consists of two primary flow circuits: one for the diluate, and the other for the concentrate. At the start of each batch process, both tanks hold feedwater at the same concentration. The relative volume of water in the diluate versus the concentrate circuits governs the recovery ratio of the process. During desalination, a voltage is applied and fluid is recirculated through the stack until the desired concentration is achieved in the diluate tank. The voltage and recirculation flowrates are held constant during this batch process, which is consistent with the work of others, both in simulation and practice [16-19], and would facilitate the simplest commercial product.

An additional circuit may be required for the electrode rinse stream; however, its design is not considered here because it is not expected to strongly affect desalination performance. Furthermore, for the hybrid ED-RO system investigated by Thampy et al., the RO reject was used to rinse the ED electrodes [10]. It may therefore be possible to integrate the rinse with the concentrate circuit to eliminate a third pump.

3. Models

The models used in this analysis have been thoroughly described and validated by Wright et al. [20]. However, a brief overview of the theory relevant to this optimization problem is presented herein to facilitate the reader's understanding of the work. For a more detailed description of the mass transfer processes in electrodialysis, Ortiz et al. [19], Strathmann [21], and Tanaka [22] also are recommended.

Following common practice, this work models desalination assuming a sodium-chloride solution. While production rates may vary for other ions, design insights obtained through this analysis are expected to remain relevant [20].

3.1. Mass transfer

Mass transfer was modeled using a similar approach as Ortiz et al. [19]. The full details are spared here. Instead, an analogous circuit (Fig. 2) is used to facilitate a discussion surrounding the principal terms affecting ion movement from the diluate to the concentrate channels.

An applied voltage V drives the movement of ions, represented by an equivalent current density i [A/m^2], through a series of diluate and concentrate channels separated by alternating cation (CEM) and anion (AEM) exchange membranes with static resistances R_{CEM} and R_{AEM} [Ω-m^2], respectively. Other ohmic resistance terms are associated with the

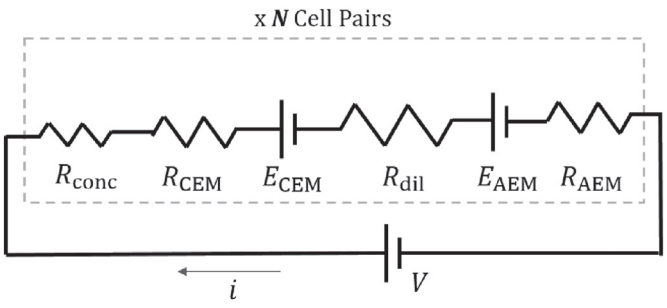

Fig. 2. ED is represented by an analogous circuit whereby ion transport is modeled by a current i due to the application of a voltage V over N cell-pairs. Exchange membranes (AEM and CEM) and channels (diluate and concentrate) are modeled using effective resistances R and back-potentials E.

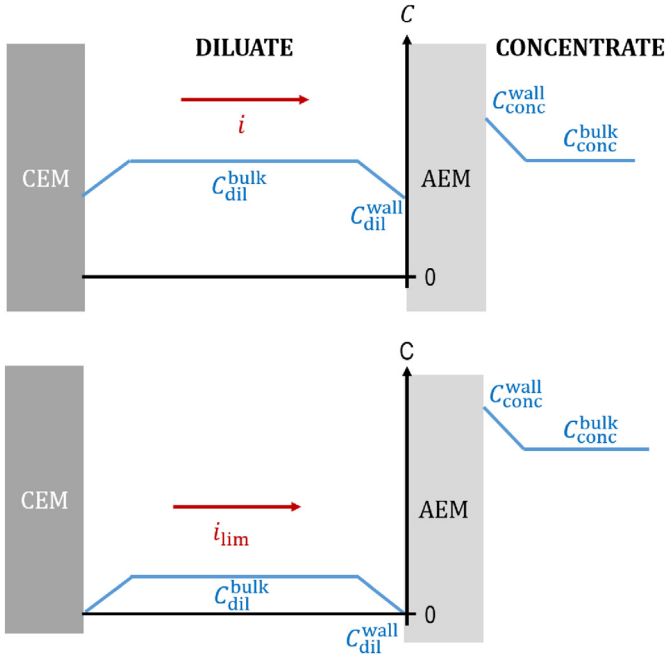

Fig. 3. Ion transfer number differences in the bulk solution and membrane produces a polarization effect, hence the concentration at the wall C^{wall} differs from the bulk C^{bulk} under an applied current density i (top). The limiting current density i_{lim} produces a zero C_{dil}^{wall}, and is a function of C_{dil}^{bulk} (bottom).

diluate and concentrate streams (R_{dil} and R_{conc}). They increase with solution resistivity ρ_s [Ω-m] and channel height h [m] as per

$$R = \rho_s h. \tag{1}$$

Finally, a back-potential develops across the membranes due to salinity differences in alternating channels and concentration polarization (Fig. 3). These terms (E_{CEM} and E_{AEM}) [V] are each modeled as

$$E_{mem} = \frac{RT}{F} \ln\left(\frac{a_{conc}^{wall}}{a_{dil}^{wall}}\right), \tag{2}$$

assuming perfect ion-selective membranes, where R is the gas constant (J/mol-K), F is Faraday's constant [C/mol], T [K] is the temperature of the solution, and the activities $a_{dil}{}^{wall}$ and $a_{conc}{}^{wall}$ are related to the wall concentrations.

The dominant impedance in brackish water desalination using ED is the resistance of the diluate channels because the resistivity increases sharply at low concentrations (Fig. 4). In addition, the high membrane potential and low limiting current were expected to drastically increase the cost of designs targeted at achieving the lowest product water concentrations.

3.2. Limiting current density

A concentration boundary layer evolves at the interface between the fluid in the channels and the membranes when a voltage is applied. As a result, the maximum rate of ion transport is bounded by a current density which produces a zero ion concentration at the membrane surface in the diluate channel (Fig. 3). This limiting current density i_{lim} [A/m^2], which plays an important role in the design of an ED stack, is estimated using

$$i_{lim} = \frac{C_{dil}^{bulk} zFk}{T_{mem} - t}, \tag{3}$$

where z is the valence of the ion, T_{mem} is the transport number of the ion in the membrane, and t is the transport number of the ion in the bulk solution where its concentration is C_{dil}^{bulk}. The boundary-layer mass

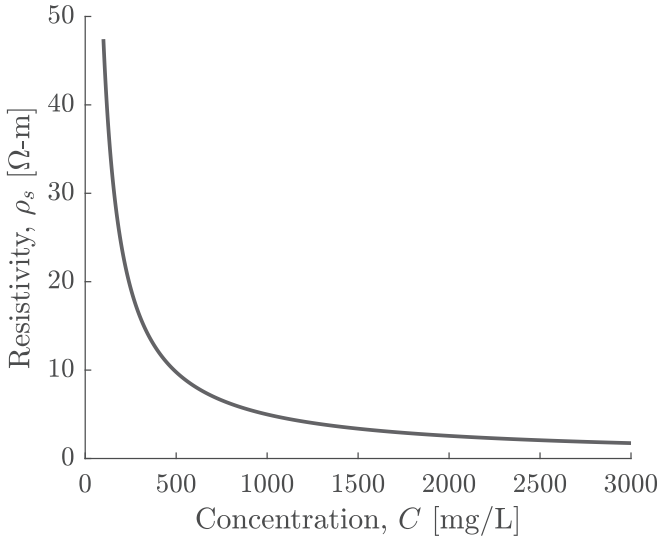

Fig. 4. Resistivity of a NaCl solution modeled using Faalkenhaagen equation [23].

transfer coefficient k [m/s] is dependent on hydrodynamic factors such as the flow-velocity, which in-turn is affected by the geometry of the ED stack and the choice of pump.

3.3. Coupling mass transfer to flow

By definition, the Sherwood Number Sh is related to k by

$$k = \frac{ShD}{d_h}. \tag{4}$$

D is the diffusion coefficient of the solution, and the hydraulic diameter d_h defined by Pawlowski et al. [24] is

$$d_h = \frac{4\varepsilon}{2/h + (1-\varepsilon)(8/h)}. \tag{5}$$

The void fraction ε is the fraction of the channel that is not occupied by the flow-spacer (Eqn. 15). The mass transfer is then correlated to the flow properties via

$$Sh = 0.29 Re_d^{0.5} Sc^{0.33} \text{ [24]}, \tag{6}$$

where the Schmidt Number Sc is a material-dependent, non-dimensional quantity, and the Reynolds Number Re_d which characterizes the flow is defined as

$$Re_d = \frac{\rho u_{ch} d_h}{\mu}, \tag{7}$$

where ρ [kg/m^3] is the density of the solution, μ [Pa-s] is the viscosity of the solution, and the velocity in the spacer-filled channel u_{ch} is calculated using Eq. (14).

From Eqs. (3)–(7), it is evident that a high linear flow velocity in the channels will produce an increase in the mass transfer coefficient and a corresponding increase in the limiting current density. Using optimization, we sought to balance these benefits against costs associated with larger pressure drops.

3.4. Pressure drop

A model derived from the computational fluid dynamics (CFD) simulations conducted by Ponzio et al. [25] was used to predict the pressure drop for each ED system permutation. This was the only model, among those evaluated by Wright et al. [20], that captured the nonlinear variation of friction factor at high velocities. Here it is sufficient to recognize that the dominant source of pressure loss is the flow

through the channels, modeled as

$$\Delta p = C_p \frac{\rho f L u_v^2}{4h}, \tag{8}$$

where $C_p = 3$ is a fitting coefficient to accommodate the difference between Ponzio et al. 's predictions, and the pressure drop measured on a bench-scale stack [20] of similar size and proportions to the designs generated for the present application. L [cm] is the length of the channel's active area, and the void channel (without spacer) velocity u_v [cm/s] is related to the volumetric flow in each circuit Q [L/ h] by

$$u_v = \frac{Q}{WhN}, \tag{9}$$

where W [cm] is the width of the active area and N is the number of cell-pairs. Then, using an alternative Reynolds Number Re definition based on the void channel velocity,

$$\mathrm{Re} = 2\frac{\rho u_v h}{\mu}, \tag{10}$$

the friction factor f is approximated from the results of Ponzio et al. [25] using the correlations

$$f = 1400/\mathrm{Re} \text{ for } \mathrm{Re} < 61, \text{and}$$
$$f = 104.5/\mathrm{Re}^{0.37} \text{ for } \mathrm{Re} \geq 61. \tag{11}$$

3.5. Flow spacer

In addition to inducing a greater pressure drop, a thinner spacer will also provide a lower area for ion transport because its filaments tend to be more closely woven. This effect is accommodated by adjusting the area by a porosity value η or 'shadow factor', calculated as

$$\eta = \frac{(l_f - d_f)^2}{(l_f)^2} \tag{12}$$

assuming an orthogonal arrangement of filaments (Fig. 5). The spacing l_f[mm] and the diameter d_f[mm] of filaments are related to the height of each channel (spacer thickness) by

$$l_f = 1.5h, \text{ and}$$
$$d_f = \frac{h}{2cf} \tag{13}$$

using a compaction factor cf of 0.946 [26]. A conservative factor of 1.5 in Eq. (13) was applied after surveying the product offerings from manufacturers of woven meshes [27,28].

Due to the presence of a flow-spacer, the actual linear flow velocity u_{ch} in the spacer is approximated from the void channel flow velocity (Eq. (9)) using

$$u_{ch} = \frac{u_v}{\varepsilon} \tag{14}$$

where the void fraction ε is defined as

$$\varepsilon = 1 - \frac{\pi d_f^2}{2 l_f h}. \tag{15}$$

We acknowledge that accurate prediction of the pressure drop and mass transfer requires consideration of several other variables including the spacer orientation, spacing and angle between filaments, and whether they are woven or not. This level of detail was not deemed necessary for this analysis, but several studies have aimed to characterize these relationships [26,29-32]. Their results could be implemented for more detailed design deliberation in the future.

4. Optimization

The optimization problem of identifying the geometry and operating parameters which provided the lowest-cost system is presented in the following section. In the primary investigation described in Sections 4.1–4.5, the feed concentration and recovery ratio are maintained at 2000 mg/L and 90%, respectively. The sensitivity to these parameters is then explored separately in a second problem formulation, which is described thereafter in Section 4.6.

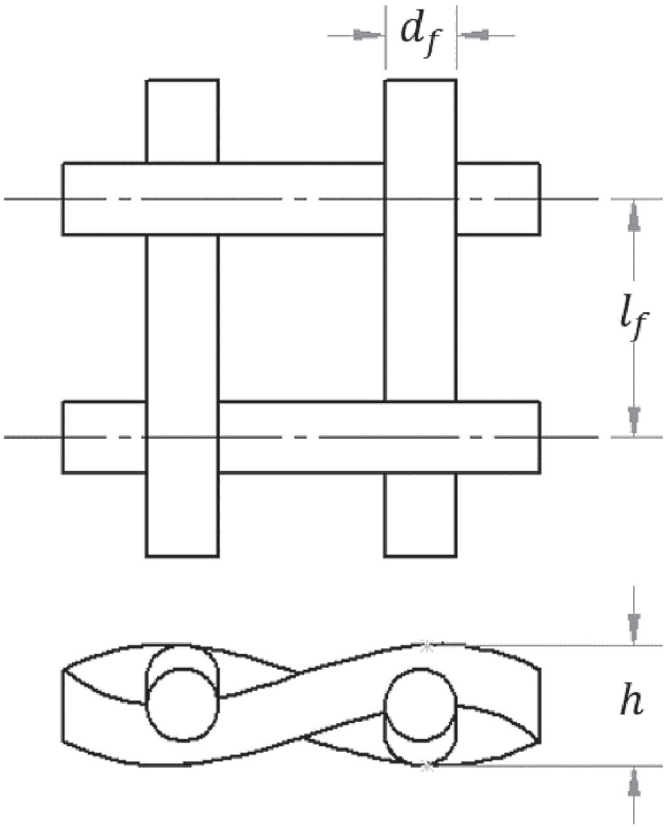

Fig. 5. Detail view of woven mesh which is often used as a spacer and turbulence promoter in the flow channels.

4.1. Problem formulation

Using standard notation, the multi-objective optimization problem is denoted as

$$\begin{aligned} \min_{\mathbf{x}} \quad & \mathbf{J}(\mathbf{x}, \mathbf{p}) \\ \text{s.t.} \quad & \mathbf{g}(\mathbf{x}, \mathbf{p}) \leq 0 \\ & \mathbf{h}(\mathbf{x}, \mathbf{p}) = 0 \\ & \mathbf{x_{lb}} \leq \mathbf{x} \leq \mathbf{x_{ub}}, \end{aligned} \tag{16}$$

where $\mathbf{x}$ is the design vector to be optimized, $\mathbf{p}$ is the vector of constant model parameters, $\mathbf{J}(\mathbf{x})$ is the vector of objective functions, and $\mathbf{g}(\mathbf{x})$ and $\mathbf{h}(\mathbf{x})$ are the inequality and equality constraints respectively. In this study, the design vector is bounded from below and above by $\mathbf{x}_{\mathbf{l}\ \mathbf{b}}$ and $\mathbf{x}_{\mathbf{u}\ \mathbf{b}}$, respectively.

4.2. Variables and bounds

Each design permutation is defined by a design vector $\mathbf{x}$ consisting of the six individual variables listed in Table 1 and illustrated in Fig. 6. The bounds for dimensional variables (L, W, and N) ensure that the proposed system could be packaged within the same envelope as existing domestic RO systems.

Channel heights (h) could vary within the size range of commonly available flow spacers. While thinner mesh thicknesses are available, they are expected to produce pressures (> 2 atm) that exceed the

Table 1
Design variables and respective bounds.

Variable	Symbol	Bounds
Length of active area	L	2–30 cm
Width of active area	W	2–20 cm
Number of cell pairs	N	10–50
Channel height	h	0.30–1.00 mm
Flow rate	Q	10–300 L/h
Voltage	V	5–100 V

capacity of commercially available small-scale pumps in the desired range of flow-rates.

Following the industry-standard operating procedure, equal flow-rates (Q) were prescribed for the diluate and concentrate circuits so that the effects of transmembrane pressure differences could be neglected in this analysis. Then, for equal diluate and concentrate channel dimensions, identical pumps could be used for both streams.

Pumps were not treated as variables. Instead, a pressure drop was calculated for each design iteration. Then, the pump (among the selection provided in Appendix A) that most closely provided the desired flow-rate served as a reference for power and cost estimation.

All variables, including the number of cell-pairs, were treated as continuous due to the limitations of the algorithm implementation (see Section 4.7). In practice, the number of cell-pairs would be rounded up to the closest integer from the value recommended by the optimizer.

4.3. Objective function

In this multi-objective optimization problem, the first objective in $\mathbf{J} = [J_1\ J_2]$ was to minimize the total cost of ownership for the proposed domestic ED system. Therefore, J_1 was defined as the total cost TC of the system, given by

$$J_1 = TC = CC + OC \tag{17}$$

where CC is the capital cost, and OC is the operating cost. While the quoted unit costs of materials assumed in this analysis likely included a profit-margin for the suppliers, the final vendor's mark-up on manufacturing cost was not considered because it is affected by commercial factors that may vary one market to another.

Since ED systems are not widely used for domestic desalination, the fouling characteristics and associated maintenance costs are not well-understood. For this reason, the operating cost considered here is only a function of the energy consumption, and given by

Table 2
Unit cost of ED stack components.

Component	Cost	Reference
Electrodes	\$2000/m^2	[34]
CEMs	\$45/m^2	[35]
AEMs	\$41/m^2	[35]
Spacers	\$3/m^2	[36]

$$OC = \mathbb{V} E_s r_E \tag{18}$$

where $\mathbb{V}$ [L] is the total volume desalinated water produced over the assumed product lifetime of 7 years, E_s [J/L] is the specific energy consumption calculated for each design permutation, and the specific cost of electrical energy r_E is approximated at \$0.10/kWh [33].

The capital cost is calculated using the rates provided in Table 2. These rates were obtained from wholesale suppliers in order to best estimate the cost at large-scale production. The capital cost for all pumps considered in this optimization study are provided in Appendix A.

We intended to capture the minimum active area that satisfied the target production rate and concentration performance. Therefore, the material forming the sealed perimeter (Fig. 6), which isolates the diluate and concentrate streams and prevents leakage, was not factored into the cost because the thickness of the seal is affected by other design and manufacturing considerations. For example, placing the tie-rods externally to the membranes may allow a thinner seal to be used.

The second objective J_2 is to maximize the rate of desalinated water production Q_p [L/h], calculated from

$$J_2 = -Q_p = -\frac{V_b r}{t_b}, \tag{19}$$

where V_b [L] is the volume in the diluate tank for each batch, r is the recovery ratio, and t_b [h] is the time to process each batch. The negative sign reflects the desire to maximize production rate.

For most simulations, the product water concentration was treated as a fixed parameter for calculating production rates of design permutations. However, some additional runs were also performed with the product concentration treated as a third objective where

$$J_3 = C_{prod}, \tag{20}$$

in order to draw generalizations regarding the effect of product water concentration C_{prod} [mg/L] on cost-optimal design.

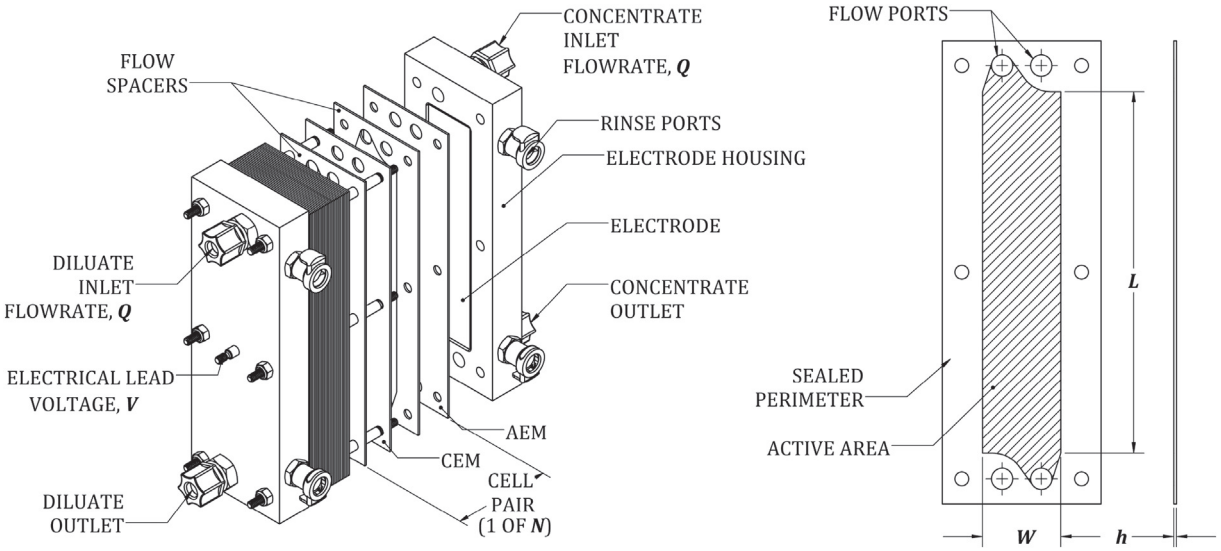

Fig. 6. Schematic of complete ED Stack (left) and individual flow-spacer (right) indicating variables considered for optimization in bold font.

4.4. Constraints

During the batch simulation, the duration t_{lim} over which the applied current density exceeded 90% (safety factor) of the instantaneous limiting current density was tracked. To ensure that designs operated under the limiting current density, the first inequality constraint in $\mathbf{g} = [g_1\ g_2\ g_3] \leq 0$ to be imposed is

$$g_1 = \frac{t_{lim}}{t_b} - 0.02, \tag{21}$$

implying that the safety factor-adjusted limiting current density could not be exceeded for more than 2% of the batch period.

Existing domestic RO products have set expectations for the production rate of desalinated water. As such, we were interested in exploring ED system designs that provided similar production rates (Q_p) in the range of 9–15 L/ h[3,4]. Therefore,

$$g_2 = 9\ \text{L/h} - Q_p \text{ and}$$
$$g_3 = Q_p - 15\ \text{L/h}. \tag{22}$$

Lastly, no equality constraints **h** were required in this formulation, making the problem easier to solve numerically.

4.5. Parameters

Parameters pertaining to the model are provided in Wright et al. [20]. Others corresponding to the cost of components and energy have been provided in Table 2. In Table 3, we provide the remaining parameters relevant to simulation.

The relative sizes of the diluate and concentrate tanks were selected to yield a recovery ratio of 90%, while the actual volumes allowed them to be packaged within the envelope of existing RO systems. The recovery ratio is maintained at 90% in the primary investigation because the purpose of the proposed device is to conserve water; however, the sensitivity to varying the recovery ratio between 60–90% is also independently explored (Section 4.6).

Solution resistivity was demonstrated to be highly sensitive to concentration changes below approximately 500 mg/L (Fig. 4); therefore, it was anticipated that the design of an ED system would be more affected by the product water requirements than the feed water concentration. As such, the feed concentration is held fixed at 2000 mg/L, based on the salinity of Indian groundwater [6], while the product concentration target is varied from 100 to 300 mg/L in the primary investigation. The latter range not only satisfies the specifications for water considered suitable for drinking according to the Bureau of Indian Standards [1], but also conforms to the palette of those who are accustomed to drinking RO-filtered water [10]. We then explore the sensitivity to the feed-water concentration separately while maintaining the product concentration at the mid-range value of 200 mg/L (Section 4.6).

$\mathbb{V}$ is calculated over the assumed product ownership lifetime of seven years, based on existing domestic RO device usage, at an average daily drinking water consumption rate of 3 L/day per person [37] for a household of five members.

Table 3
Simulation parameters for primary investigation, results in Section 5.

Parameter	Value
Feed concentration, C_{feed}	2000 mg/L
Product concentration, C_{prod}	100–300 mg/L
Recovery ratio, r	90%
Diluate tank volume, $\mathbb{V}_{dil}$	3.6 L
Concentrate tank volume, $\mathbb{V}_{conc}$	0.4 L
Total volume produced, $\mathbb{V}$	38,325 L

Table 4
Simulation parameters for sensitivity analysis, results in Section 6.

Parameter	Value
Feed concentration, C_{feed}	1500–2500 mg/L
Product concentration, C_{prod}	200 mg/L
Recovery ratio, $\mathbb{V}_{dil}$	60–90%
Diluate tank volume, $\mathbb{V}_{dil}$	3.6 L
Concentrate tank volume, $\mathbb{V}_{conc}$	2.4–0.4 L
Total volume produced, $\mathbb{V}$	38,325 L

4.6. Sensitivity analysis

Sensitivity to the feed concentration and recovery was additionally investigated over a range of 1500–2500 mg/L and 60–90%, respectively. Here, the product water concentration was maintained at 200 mg/L with a targeted production rate of 12 ± 0.5 L/ h. The objective and constraint functions expressed in Eqs. (19) and (22) were correspondingly modified such that

$$J_2 = -C_{feed}, \tag{23}$$

$$g_2 = 11.5\ \text{L/h} - Q_p, \text{and}$$
$$g_3 = Q_p - 12.5\ \text{L/h}. \tag{24}$$

To model the changing recovery ratio, the concentrate tank volume was increased from 0.4 L at a recovery of 90%, to 2.4 L at a recovery of 60%, while the diluate tank volume was maintained at 3.6 L in all cases (Table 4).

4.7. Simulation and optimizer

The block diagram in Fig. 7 approximates the optimization process, which was implemented in MATLAB [38]. Conventional gradient-based algorithms could not be applied with this formulation because the discrete selection of pumps caused the solution to converge at local minima. Instead, the problem described above was solved using a multi-objective genetic algorithm, specifically the modified NSGA-II algorithm [39] implementation in MATLAB. The solution is a set of non-dominated Pareto optimal solutions with respect to the problem objective functions. The difference between the original NSGA-II [40,41] and the modified version is that the modified version adds an extra tuning parameter, Pareto Fraction (PF∈ (0,1)), to control the number of elite members in each population that progress to the next generation. By testing different PFs, we determined that values between 0.5 to 0.75 provided non-dominated solutions without sacrificing convergence speed.

5. Results and discussion

In this section, cost-optimal designs obtained for varying production rate and product concentration requirements are first discussed at a fixed feed concentration and recovery ratio of 2000 mg/L and 90%, respectively.

5.1. Capital cost vs total cost

Optimal designs that minimized total cost were similar in cost and design to those that minimized capital cost. For example, Fig. 8 compares the total cost for designs which produce 200 mg/L product water at varying production rates, optimized either for minimum total cost or for minimum capital cost. The former objective function did indeed provide a lower total cost compared to the latter, but the difference of ~$5 was negligible.

This result is explained by comparing the contributions from the operating and the capital cost (Fig. 9). The operating cost is significantly lower than the capital cost because the cost of electrical

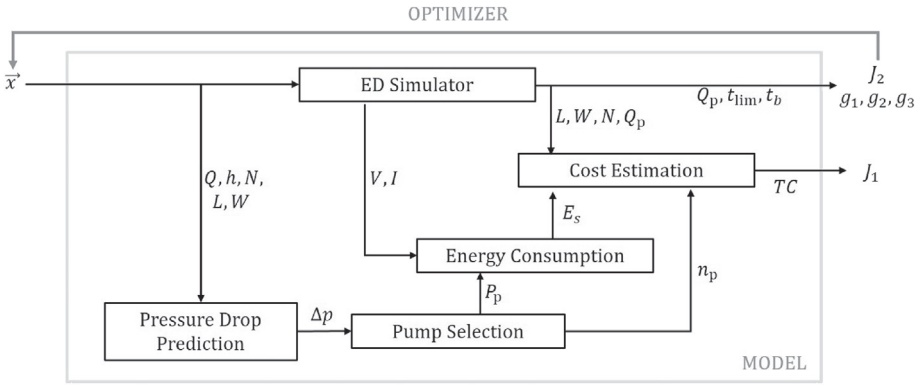

Fig. 7. Block diagram indicating the flow of design variables between models to calculate the objective function for optimization.

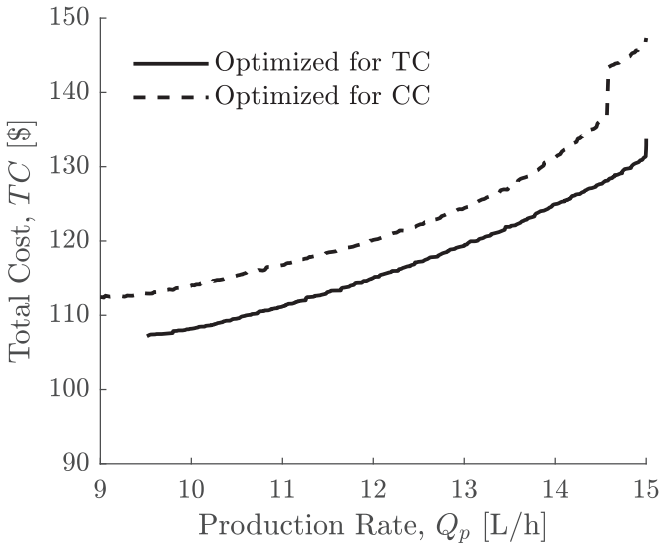

Fig. 8. Designs optimized for minimum capital cost (CC) had similar total costs to those optimized for minimum total cost (TC) for varying production rates at 200 mg/L product concentration.

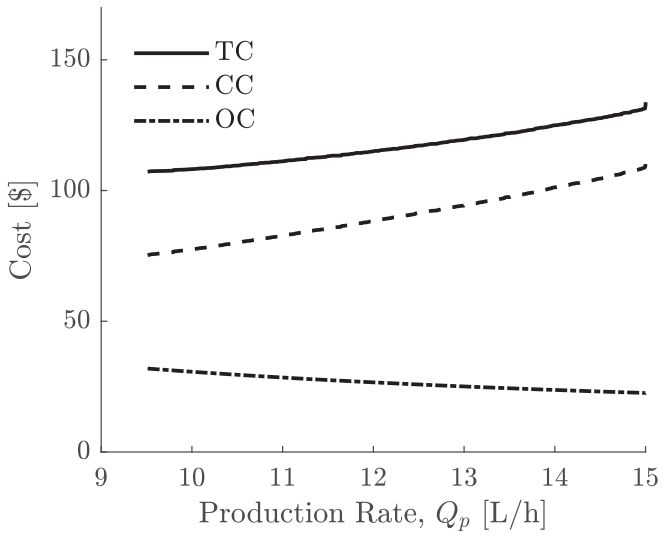

Fig. 9. The operating cost (OC) is lower than the capital cost (CC) for designs optimized for producing 200 mg/L product water at varying production rates.

energy is small compared to equipment costs, and the system is utilized infrequently. In domestic applications, the system will only be used for 1–2 hours per day depending on the drinking water requirements of the household.

The design of an affordable domestic ED system is therefore concerned with capital cost minimization. The reader is reminded that this result was obtained even without the inclusion of a mark-up on the capital cost of the system.

5.2. Current density

The increasing capital cost, and decreasing operating cost, with production rate (Fig. 9) are explained by examining the current density during the operation of the cost-optimized designs.

5.2.1. Maximization of current density

It was established in Section 3 that in brackish water electrodialysis, the dominant resistance is associated with diluate channels. Since this term is ohmic in nature, the power consumption at a fixed ion removal rate is expected to increase approximately with i^2, where i is the current density. Subsequently, to the first order

$$OC \propto i^2. \tag{25}$$

However, the required cross-sectional area at the same ion removal rate decreases as

$$CC \propto 1/i. \tag{26}$$

Since it has been established that the capital cost - which scales primarily with active area (Table 2) - is the dominant term in the total cost, optimal domestic ED designs are therefore expected to maximize current density. To verify this hypothesis, we examined the ratio of the applied current density to the limiting current density (adjusted by the safety factor $n_s = 0.9$) when the desired product water concentration was achieved (Fig. 10). This ratio approaches 1 for all optimal designs over the range of product water concentrations (100–300 mg/L), thereby confirming the aforementioned expectation.

These results agree with McGovern et al. and Chehayeb et al.'s findings that maximization of current density is cost-optimal for brackish water ED desalination at high equipment-to-energy cost ratios [12,42].

5.2.2. Limiting current density implications

Maximizing the current density is cost-optimal, but there is an upper bound based on the instantaneous diluate concentration and the flow properties (Section 3.2). Fig. 10 demonstrates that the applied current density approaches this limit at the *end* of each batch; however, it is also useful to examine the full duration.

For example, the optimal current trajectories during desalination for producing 100 mg/L and 200 mg/L product water at a rate of 10 L/h are compared in Fig. 11. Since the **limiting** current density trajectories

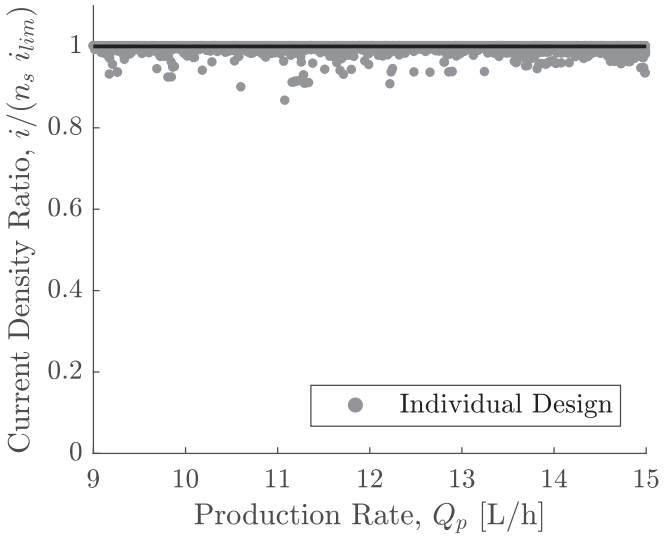

Fig. 10. Ratio of instantaneous applied current density i to limiting current density i_{lim} at the end of the batch process approaches 1 for all optimum designs targeted at varying product concentrations (100–300 mg/L) and production rates (9–15 L/h).

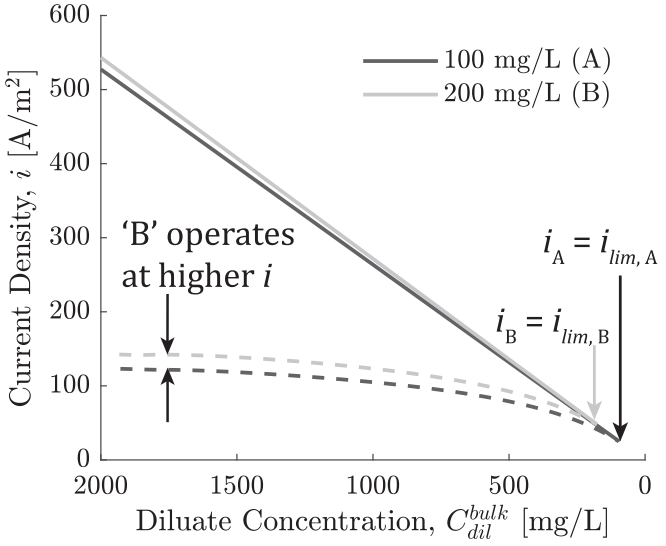

Fig. 11. Simulated applied (dashed lines) and limiting (solid) current densities through desalination for designs optimized to produce 200 and 100 mg/L water at 10 L/h.

(solid lines) are similar and mostly dependent on the instantaneous diluate concentration, it is inferred that differences in flow characteristics play a small role here. These upper bounds are only approached at the end of the batch, but application of a constant voltage constrains the full **applied** current trajectory. Therefore, as is evident in Fig. 11, relaxation of the product water requirements allows designs to operate at higher current densities for the full batch process.

To further understand the implications of this behavior on cost (Fig. 12), we examined the time-averaged applied current densities $\bar{i}$ during the operation of optimal designs. The following insights were obtained:

1. With the exception of a few outliers, optimized designs agree with the approximate scaling relationships for the capital cost *CC* and operating cost *OC* presented in Eqs. (25) and (26). The y-intercept for the *OC* trend-line approximates the energetic cost of pumping.
2. By extrapolating the *CC* and *OC* trend-lines beyond the optimization data, it is speculated that a time-averaged current density $\bar{i}$ of approximately 235 A/m^2 will yield an absolute minimum total cost, which in turn is a function of the specific material and energy costs.
3. Despite the use of optimization, designs targeted at the product concentrations of 100–300 mg/L, at the production rates of interest, lie in the capital cost-dominated region. Hence, the absolute minimum cost could be achieved by relaxing the product water concentration requirements.
4. Due to the upper bound on $\bar{i}$ imposed by i_{lim}, designs targeted at lower concentrations C_{prod} are further from the absolute minimum cost. Therefore, relaxing the product water requirements allows operation at higher current densities, hence lowering total cost.
5. Scatter in the data about the trend-lines represents varying production rate requirements. The gradient indicates that increasing the production rate requirements Q_p from 9 to 15 L/h also forces operation at lower $\bar{i}$, albeit to a lesser extent than decreasing the product water concentration requirement from 300 to 100 mg/L. As a result, achieving higher production rates also requires an increase in cell-pair area, thereby increasing capital cost. This increase in capital cost exceeds the decrease in operating cost obtained by operating at a lower current density; therefore total cost increases with production rate.
6. The ability to produce low product water concentrations that are comparable to RO (100 mg/L) comes at a significant economic cost. It may be worthwhile to investigate if users would accept product water at higher salinities of 200 to 300 mg/L, which is still suitable for drinking but decreases the system cost significantly.
7. In order to further improve affordability of the proposed batch domestic ED system, the two options are to decrease the unit cost of the components (shifting the *CC* line down), or to find methods for operating at higher time-averaged current densities (shifting points to the right).

By analyzing Figs. 11 and 12, we discovered that $\bar{i}$ can be increased with time-varying voltage regulation based on measured conductivity of the diluate stream. A high voltage can be applied at the start of the batch process and be gradually decreased to maintain an instantaneous current density that is just under the limiting current density (see Fig. 11). Since this strategy has the potential to provide significant cost reductions, it is an avenue of ongoing work for our team.

5.3. Optimal design characterization

In order to minimize capital and total cost of a domestic ED system, it has been shown that the optimal strategy is to maximize the applied current density. We explored how this strategy affected the choice of variable values in order to provide design guidance.

5.3.1. Linear flow velocity, u_{ch}

The linear velocity is reported instead of the volumetric flow rate because it is more directly applicable to design, and comparable between different scales of production. Optimal designs operated at 18–21 cm/s for 300 mg/L, 15–18 cm/s for 200 mg/L, and 11–16 cm/s for 100 mg/L product water (Fig. 13a). These results exceed typical values used by others in both experimental and theoretical studies, including Lee et al. (7.5 cm/s) [14], Tanaka (10 cm/s) [16], and Kim et al. (4.24 cm/s) [43]. However, they agree well with Chehayeb et al. who calculated an optimum velocity of 16–18 cm/s for ED desalination from 3000 mg/L to 350 mg/L in a continuous system. We postulate that the suggested high linear velocities are not implemented in practice, because the resulting pressures may be difficult to manage for larger systems. Furthermore, a lower velocity may be desirable for continuous systems in order to increase the residence time of the solution and provide greater concentration reduction. As a result, little work has been performed to understand the effect of high flow velocities on desalination performance, fouling behavior, and membrane durability.

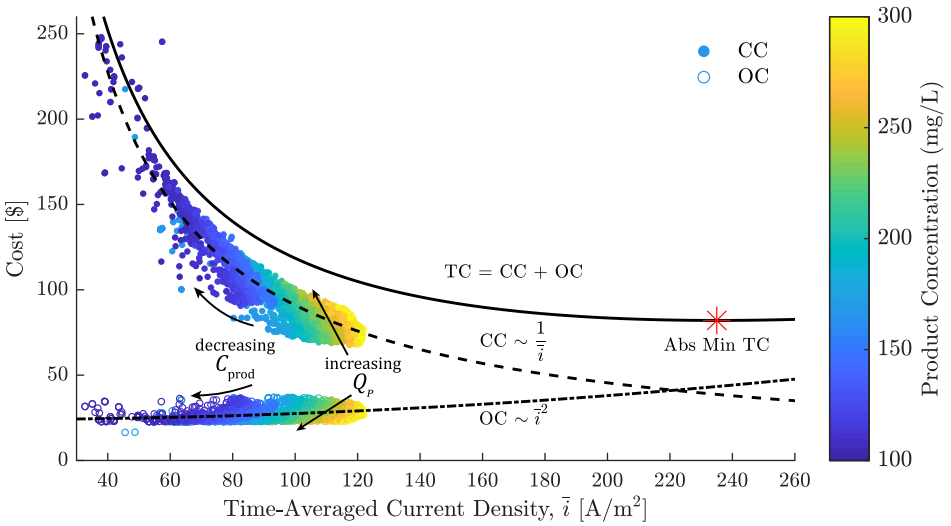

Fig. 12. Capital cost *CC* and operating cost *OC* for optimal designs is plotted against the time-averaged current density $\bar{i}$ during their respective batch operation. Straight and curved arrows indicate direction of increasing production rate Q_p (9 to 15 L/h) and decreasing product water concentration C_{prod} (300 to 100 mg/L), respectively. Desalination was simulated for 2000 mg/L feed at 90% recovery.

This work suggests that the development of domestic ED systems may benefit from characterization of these effects.

The decrease in the linear flow velocity with the production rate is explained by the increase in the cell-pair area. The volume flow-rate per cell pair remained approximately constant at 5.1 ± 0.1 L/h for the 200/300 mg/L and 6.0 ± 0.2 L/h for 100 mg/L, utilizing the maximum capacity of the small-scale pumps used in this investigation. Then, as the width of the active area grew to satisfy higher production rates, the linear velocity decreased.

5.3.2. Voltage, V

In order to avoid exceeding the the limiting current density at the end of the batch, the applied voltage was smaller for designs that targeted lower product water concentrations (Fig. 13b). Furthermore, the decrease in the applied voltage observed at higher production rates is explained by the decreasing linear flow velocities. Optimal voltage values, ranging between 0.7–1.3 V per cell-pair, agreed with other studies and manufacturer recommendations for concentration ranges similar to those investigated here [11,16,19,44].

5.3.3. Cell-pair area, LW

Larger cell-pair area is required to provide the required salt removal rate while compensating for the decrease in the applied voltage (and associated current) at lower concentrations and higher production rates (Fig. 13c). Both length and width increased with production rate, but the former increased at a faster rate. Inspection of the aspect ratio, defined as *L/W* (Fig. 13d), indicates that leaner designs are better-performing because they supply a higher linear flow velocity for a given cell-pair area, thereby facilitating operation at higher current densities, provided that the pumps can sustain the resulting pressure drop. For the 100 mg/L case, a decrease in the aspect ratio was observed after 12 L/h because the length was prevented from exceeding the upper bound of 30 cm.

Recall that the membrane and spacer material contribution to the seal is not factored into the cost. In practice, implementation of a thick seal will decrease the optimum *L/W* aspect ratio.

5.3.4. Capital cost, CC

Capital cost of optimal systems increased nonlinearly with decreasing product water concentration. The difference between 200 mg/L and 100 mg/L systems was greater than from 300 mg/L to 200 mg/L (Fig. 13f). The sharp increase in the diluate resistance paired with the decrease in the limiting current density with decreasing concentration explains this result. Thus, ED stack architectures targeted at low product concentrations are forced to operate at low current densities applied over larger surface areas to maintain the desired rate of salt removal. These results agree with other work that has found ED to be expensive process for producing ultra-pure water [42,45].

5.3.5. Number of cell-pairs, N

Implementing more cell-pairs to achieve a higher production rate is not necessarily cost-optimal at the domestic scale (Fig. 13e). Instead, it was found that the optimal number of cell-pairs was determined by the capacity of the selected pumps and the required linear flow velocity in the channels.

5.3.6. Channel heights, h

Smaller intermembrane channel heights decrease the electrical resistance of the channels (Eq. (1)) and increase the mass transfer coefficient (Eqs. (4)–(6)). Optimum heights approached the lower bound of the variable, ranging between 0.30 –0.33 mm for the full spectrum of production rates and concentrations analyzed in this study, and agrees with the channel height minimization observed by Chehayeb et al. in their optimization study [12], which also acknowledges the important role of pumping in brackish water ED. This result signifies that the enhanced mass transport provided by thin channels justified the cost of greater pressure drop over the design space and range of operation considered for this application.

5.4. Cost & energy breakdown

Fig. 14 distributes the capital cost of optimal systems providing between 11.5 and 12.5 L/h of production into average contributions from components. Pumps accounted for a significant fraction, particularly at 200 and 300 mg/L. The remainder was balanced between electrodes and membranes.

Comparison across the concentrations indicates that there is a significant economic penalty for producing water at the lowest salinity of 100 mg/L. Again, this observation suggests that it may be prudent to reassess user's reception toward 300 mg/L water and whether their preference for 100 mg/L justifies the significant cost addition.

A similar breakdown is provided for energy consumption due to desalination and pumping (Fig. 14). Here, pumps accounted for as high as 83% of the total energy consumption. In addition, the contribution

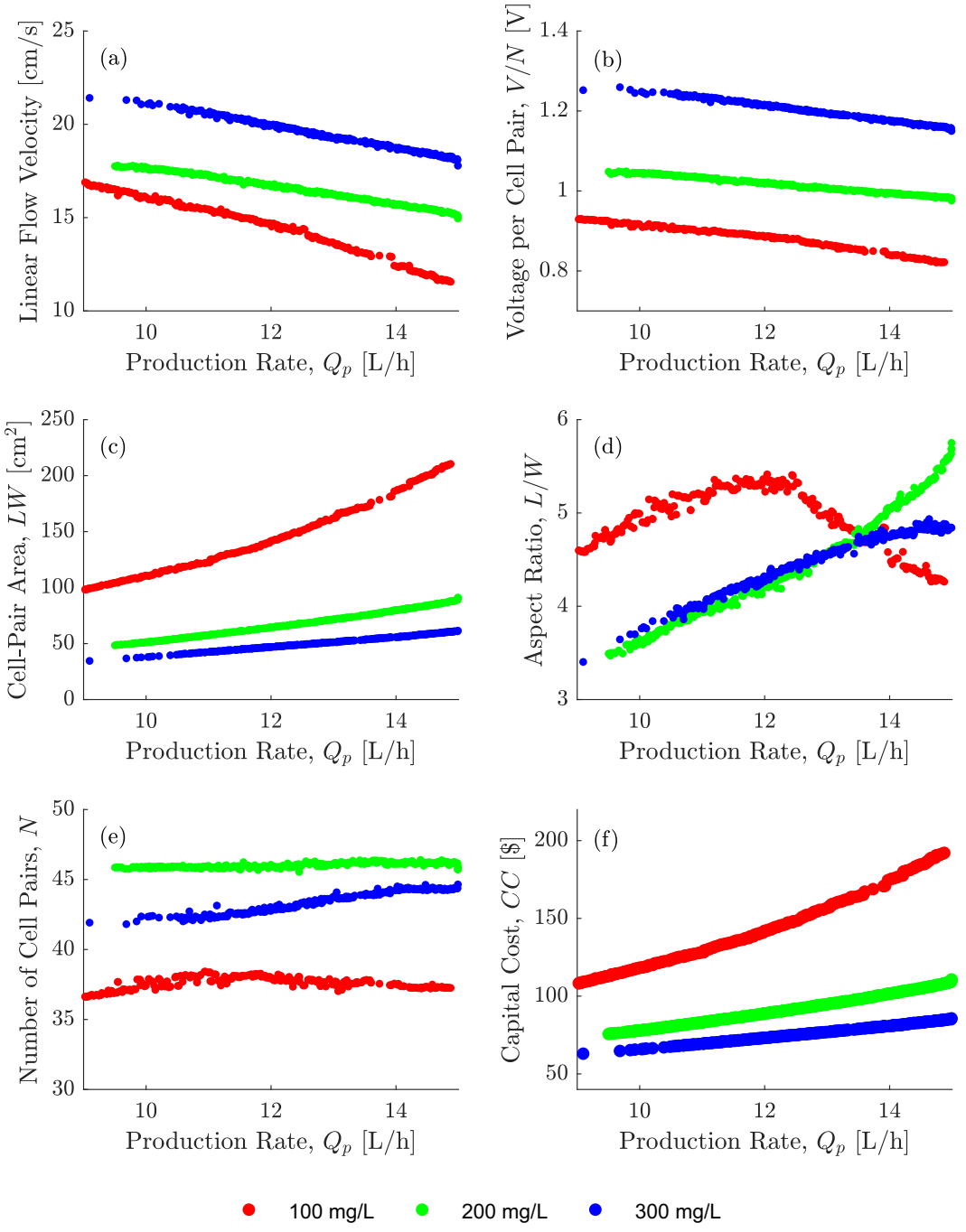

Fig. 13. Optimal selection of the design variables as a function of the production rate and concentration requirements (a–e). Pareto-optimal capital cost versus production rate for varying product water concentrations (f).

from desalination did not vary significantly with product concentration, hence mirroring the slow growth of *OC* with $\bar{i}$ in Fig. 12.

Overall, this work has indicated that the development of low-cost and energy efficient pumps that are suitable for flow-rates ranging between 200 and 300 L/ h, while sustaining pressures up to 2 bar, will assist the commercialization of domestic ED systems. In addition, a more detailed investigation surrounding the optimal geometry of flow-spacers may provide similar or better mass transfer behavior at a lower pressure drop, thereby also reducing the pumping expense.

6. Sensitivity to feed concentration & recovery ratio

In the previous section, the detailed design of an ED stack is investigated for a fixed feed concentration and recovery ratio of 2000 mg/L and 90%, respectively. Now we consider how the optimal design is affected when the feed concentration and recovery ratio are varied while the product concentration and production rate are maintained at 200 mg/L and within 12 ± 0.5 L/ h, respectively.

6.1. Total cost, TC

Between 60–90 % range, recovery ratio was evaluated to have a minimal effect on total cost (Fig. 15), because the diluate resistance is the dominant impedance in brackish water ED desalination, and is independent of recovery ratio (Section 3.1). Instead, the small maximum cost difference of $9, between 60 and 90% recovery at 2250 mg/L feed,

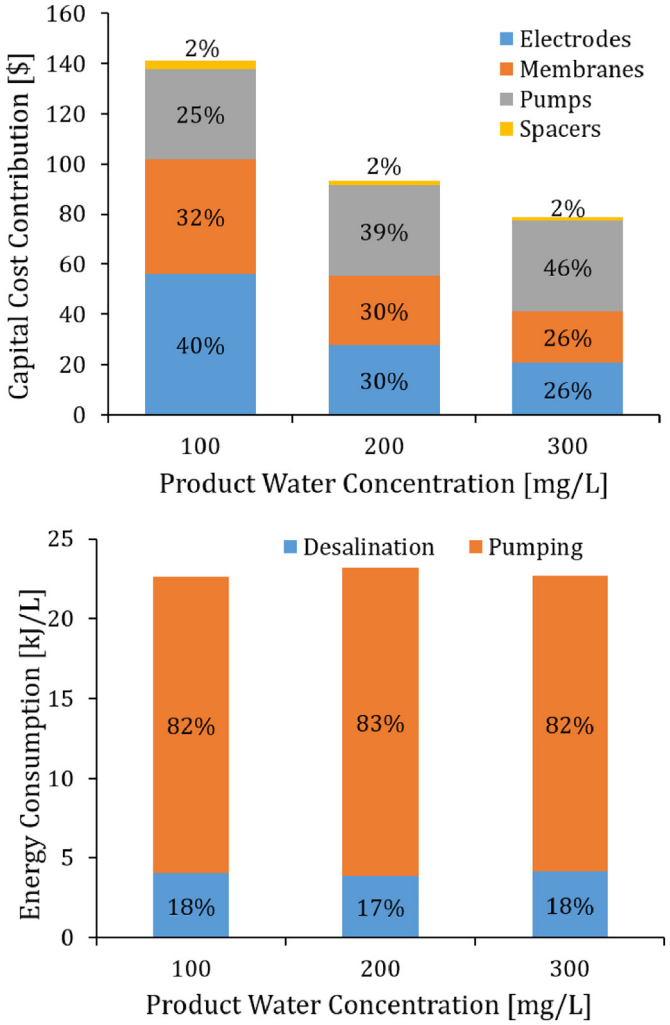

Fig. 14. Average capital cost breakdown (*top*) and desalination vs. pumping energy comparison (*bottom*) for all optimal systems producing 12 ± 0.5 L/h at different product concentrations.

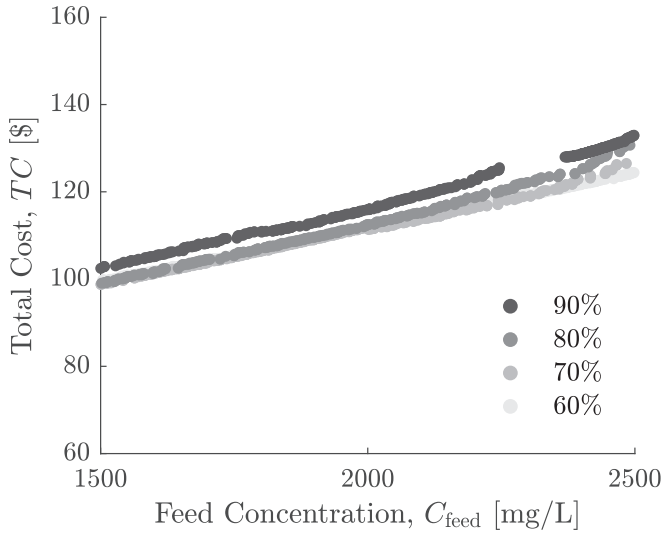

Fig. 15. Total cost of designs optimized for varying recovery ratios and feed concentrations, while maintaining a fixed product water concentration of 200 mg/L and production rate of 12 ± 0.5 L/h.

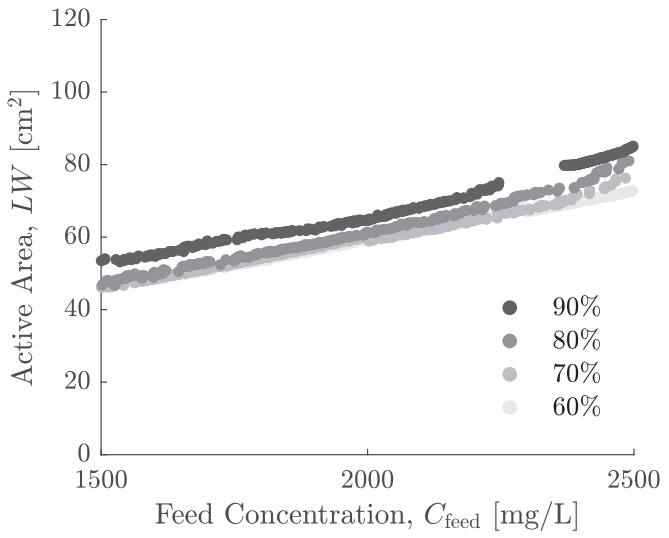

Fig. 16. Optimal active area, *LW*, plotted against feed concentration for varying recovery ratios. Desalination was simulated for a fixed product concentration of 200 mg/L and production rates of 12 ± 0.5 L/h.

is attributed to the membrane back-potential term. This term grows as a consequence of the ratio of concentrate to diluate concentration increasing with recovery ratio (Eq. (2)).

6.2. Active area, LW

The cell-pair area required for desalination increased linearly with feed concentration (Fig. 16), thereby explaining the rising total cost. Note that increasing the feed concentration has a similar effect to increasing the production rate in the primary investigation (Fig. 13c) because it requires a greater quantity of salt is to be extracted without changing the product concentration target.

6.3. Voltage per cell-pair, V/N

The reader is reminded that the maximum applied voltage is constrained by the product concentration in a conventional constant-voltage batch process (Section 5.2.2). Therefore, optimal voltages across different feed concentrations and recoveries are expected to remain comparable to the optimal ~1 V/cell-pair value obtained previously when the product water concentration was 200 mg/L (Fig. 13b). The sensitivity results matched expectations, where optimal voltages ranged between 0.93–1.06 V/cell-pair for the simulated range of feed concentrations (Fig. 17).

6.4. Linear flow velocity, u_{ch}

The optimal voltage decreased with increasing feed concentration, because the linear flow velocity decreases as the cell-pair area increases (Fig. 18). The resulting velocities of 14–19 cm/s still exceed most comparisons drawn from other literature (Section 5.3.1). Furthermore, the occurrence of the same high flow velocities at other feed concentrations and recoveries reinforces the need for characterizing the impact of high flow velocities on membrane performance.

6.5. Aspect ratio, L/W, & channel height, h

Optimal length-to-width (*L/W*) aspect ratios ranged between 3.9–5.1 for all recovery ratios and feed concentrations. These values agree with the 3.5–6 range previously calculated for desalinating from a fixed feed of 2000 mg/L to 100–300 mg/L at 9–15 L/ h(Fig. 13d). Similarly, optimal channel heights of 0.30–0.35 mm in this sensitivity

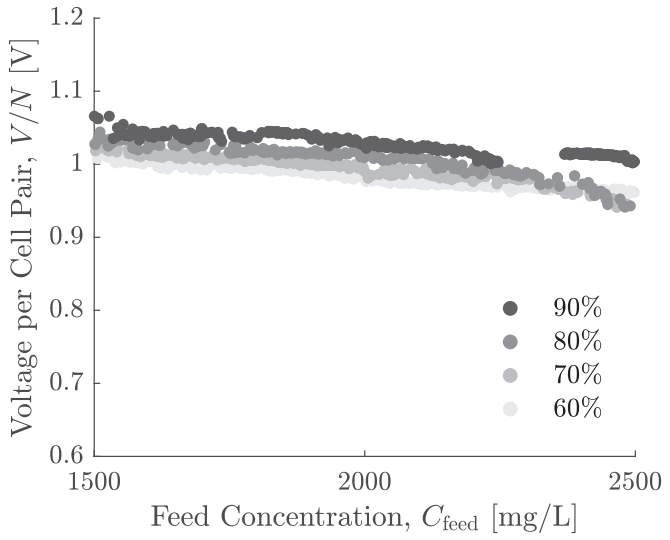

Fig. 17. Optimal applied voltage per cell-pair, *V/N*, plotted against feed concentration for varying recovery ratios. Desalination was simulated for a fixed product concentration of 200 mg/L and production rates of 12 ± 0.5 L/h.

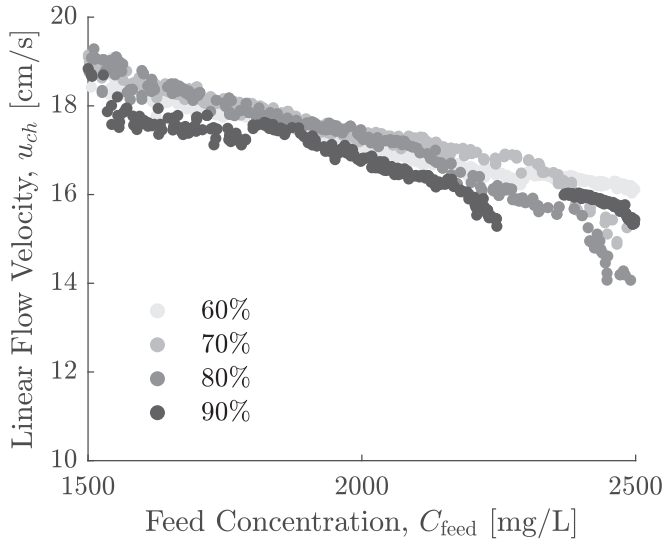

Fig. 18. Linear flow velocity, u_{ch}, plotted against feed concentration for varying recovery ratios. Desalination was simulated for a fixed product concentration of 200 mg/L and production rates of 12 ± 0.5 L/h.

analysis also approached the lower limit of 0.30 mm. Together, these results provide useful design guidance: large *L/W* cell-pair aspect ratios of 3–6, and thin channels approaching 0.35 mm or lower in height, provide a cost-optimal arrangement for domestic ED desalination over a broad range of brackish water feeds, recovery ratios, and product concentrations.

7. Conclusions

Cost-optimal designs of batch ED systems targeted at production rates of 9–15 L/h and product concentrations of 100–300 mg/L, from a fixed feed concentration of 2000 mg/L at 90% recovery, were first investigated. Voltage and flow-rates were held constant during the batch desalination process for each design.

In all cases, capital cost was found to dominate over the operating cost due to the upper-bound on the ion removal rate imposed by the limiting current density. Furthermore, capital cost was found to be sensitive to the target product water concentration such that while batch ED can be used to produce 100 mg/L water, the respective optimal designs were significantly more expensive than alternatives targeted at 200 and 300 mg/L.

Thin channels (0.30–0.33 mm), high aspect ratios (3.5 – 6), and cell-pair numbers that varied from 36 to 46 were recommended to minimize cost. Voltages applied to larger systems were found to be applicable at the domestic scale; however, optimal flow velocities (11–21 cm/s) were greater than reported in other literature.

Evaluating the sensitivity of the cost-optimal parameters at a fixed 200 mg/L product and 12 ± 0.5 L/h production rate, it was found that the active area scaled linearly with feed concentration (1500–2500 mg/L) while recovery ratio (60–90%) had minimal effect on the design and total cost.

By analyzing the limits of the optimized designs we have also identified three directions that can further increase affordability to facilitate commercialization: voltage regulation during the batch process, development of inexpensive pumps suited to this application, and a detailed investigation on optimal spacer geometry.

The primary limitation of this work is the exclusion of membrane replacement expenses in the operating cost. Since the cost-optimal approach was to minimize cell-pair area, the corresponding membrane replacement cost would also be therefore minimized. However, operating at the suggested high linear flow velocities may negatively impact membrane life, and subsequently increase replacement frequency. Therefore, further experimental work to characterize membrane performance is also recommended.

Acknowledgement

This work was supported by the Tata Center for Technology and Design at MIT and Eureka Forbes Ltd. We also thank Professor Olivier L. de Weck for providing guidance and feedback on the optimization tasks.

Appendix A. Pump selection

A system pressure-flow curve was produced for each design iteration and compared to 13 DC pump curves (Fig. A.19). With the exception of a–d which are centrifugal pumps, the remainder are diaphragm pumps. The pump, whose intersection point with the system curve most closely provided the design flow-rate, was used for estimating the cost and energy consumption. The pumps were assumed to be operating at their rated power consumption through the full batch duration.

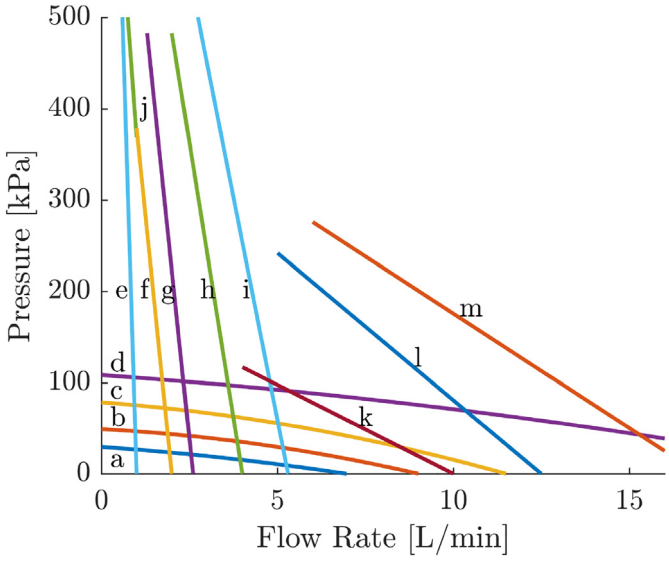

Fig. A.19. Pressure-flow relationship of pumps considered in this analysis. See Table A.5 for specifications and cost.

Table A.5
Cost and power specifications for pumps.

#	Manufacturer	Model	Power [W]	Cost [$]
a	Topsflo	B10H-B12	11	18
b	Topsflo	B04H	20	19
c	Topsflo	B10-B24	31	19
d	Topsflo	C01-B24	48	45
e	Singflo	100GRO	24	14
f	Singflo	FL-2401	22	16
g	Singflo	FL-2403	24	16
h	Singflo	FL-2402A	31	18
i	Ronda	DP-150	40	54
j	Ronda	DP-130	15	53
k	Singflo	FL-31	36	33
l	Singflo	FL-34	60	34
m	Singflo	FL-44	134	35

References

[1] Bureau of Indian Standards, Drinking Water Specification (second revision), (2012).
[2] Comprehensive Initiative on Technology Evaluation, Household Water Filter Evaluation, (2015), pp. 1–31.
[3] KENT RO Systems Ltd, Supreme RO, (2016).
[4] Eureka Forbes, Aquaguard Geneus, (2016).
[5] Transparency Market Research, Water Purifier Market - India Industry Analysis, Size, Share, Growth, Trends and Forecast 2016–2024, tech. rep. 2016 Albany, NY.
[6] N.C. Wright, A.G. Winter V, Justification for community-scale photovoltaic-powered electrodialysis desalination systems for inland rural villages in India, Desalination 352 (2014) 82–91.
[7] B. Pilat, A case for electrodialysis, Int. Water Irrig. 7 (1991) 195–225.
[8] REvivED Water Consortium, Low Energy Solutions for Drinking Water Production by a Revival of Electrodialysis Systems, (2016).
[9] B. Pilat, Practice of water desalination by electrodialysis, Desalination 139 (1–3) (2001) 385–392.
[10] S. Thampy, G.R. Desale, V.K. Shahi, B.S. Makwana, P.K. Ghosh, Development of hybrid electrodialysis-reverse osmosis domestic desalination unit for high recovery of product water, Desalination 282 (1418) (2011) 104–108.
[11] K.G. Nayar, P. Sundararaman, J.D. Schacherl, C.L. O'Connor, M.L. Heath, M.O. Gabriel, S.R. Shah, N.C. Wright, A.G. Winter V, Feasibility study of an electrodialysis system for in-home water desalination in urban India, Dev. Eng. 2 (2016) 38–46.
[12] K.M. Chehayeb, D.M. Farhat, K.G. Nayar, J.H. Lienhard, Optimal design and operation of electrodialysis for brackish-water desalination and for high-salinity brine concentration, Desalination 420 (June) (2017) 167–182.
[13] R.K. McGovern, S.M. Zubair, J.H. Lienhard V, Design and optimization of hybrid ED-RO systems for the treatment of highly saline brines, International Desalination Association World Congress, 2013 (Tianjin, China).
[14] H.J. Lee, F. Sarfert, H. Strathmann, S.H. Moon, Designing of an electrodialysis desalination plant, Desalination 142 (3) (2002) 267–286.
[15] F.S. Rohman, N. Aziz, Optimization of batch electrodialysis for hydrochloric acid recovery using orthogonal collocation method, Desalination 275 (1–3) (2011) 37–49.
[16] Y. Tanaka, A computer simulation of batch ion exchange membrane electrodialysis for desalination of saline water, Desalination 249 (3) (2009) 1039–1047.
[17] J. Uche, F. Círez, A.A. Bayod, A. Martínez, On-grid and off-grid batch-ED (electrodialysis) process: simulation and experimental tests, Energy 57 (2013) 44–54.
[18] L.J. Banasiak, T.W. Kruttschnitt, A.I. Schäfer, Desalination using electrodialysis as a function of voltage and salt concentration, Desalination 205 (1–3) (2007) 38–46.
[19] J.M. Ortiz, J.A. Sotoca, E. Expósito, F. Gallud, V. García-García, V. Montiel, A. Aldaz, Brackish water desalination by electrodialysis: batch recirculation operation modeling, J. Membr. Sci. 252 (1-2) (2005) 65–75.
[20] N.C. Wright, S.R. Shah, S.E. Amrose, A.G. Winter V, A robust model of brackish water electrodialysis desalination with experimental comparison at different size scales, Desalination (2018), http://dx.doi.org/10.1016/j.desal.2018.04.018 In Review.
[21] H. Strathmann, Electrodialysis, a mature technology with a multitude of new applications, Desalination 264 (3) (2010) 268–288.
[22] Y. Tanaka, Ion Exchange Membrane Electrodialysis: Fundamentals, Desalination, Separation, Nova Science Publishers, 2010.
[23] G. Kortüm, Treatise on Electrochemistry, Elsevier Publishing Company, 1965.
[24] S. Pawlowski, J.G. Crespo, S. Velizarov, Pressure drop in reverse electrodialysis:

experimental and modeling studies for stacks with variable number of cell pairs, J. Membr. Sci. 462 (2014) 96–111.
[25] F.N. Ponzio, A. Tamburini, A. Cipollina, G. Micale, M. Ciofalo, Experimental and computational investigation of heat transfer in channels filled by woven spacers, Int. J. Heat Mass Transf. 104 (2017) 163–177.
[26] M. Johannink, K. Masilamani, A. Mhamdi, S. Roller, W. Marquardt, Predictive pressure drop models for membrane channels with non-woven and woven spacers, Desalination 376 (2015) 41–54.
[27] CONWED Global Netting Solutions, Reverse Osmosis Feed Spacers, (2016) Minneapolis, USA.
[28] Industrial Netting, Woven Nylon, Polyester, or Polypropylene Plastic Mesh, (2016) Minneapolis, USA.
[29] G. Belfort, G.A. Guter, Hydrodynamic Studies for Electrodialysis, tech. rep. McDonnell Douglas Corporation, Newport Beach, California, 1969.
[30] G. Schock, A. Miquel, Mass transfer and pressure loss in spiral wound modules, Desalination 64 (C) (1987) 339–352.
[31] C.P. Koutsou, S.G. Yiantsios, A.J. Karabelas, Direct numerical simulation of flow in spacer-filled channels: effect of spacer geometrical characteristics, J. Membr. Sci. 291 (1–2) (2007) 53–69.
[32] L. Gurreri, A. Tamburini, A. Cipollina, G. Micale, M. Ciofalo, Flow and mass transfer in spacer-filled channels for reverse electrodialysis: a CFD parametrical study, J. Membr. Sci. 497 (2016) 300–317.
[33] Reliance Energy, MERC Multi Year Tariff Order for FY 2016-17 to FY 2019-20, Tech. Rep. (2016).
[34] Baoji Changli Special Metal Co. Ltd, Platinized Titanium Anode, (2014) Shaanxi, China.
[35] Hangzhou Iontech Environmental Co. Ltd, IONSEP Membranes, Zhejiang, China, 2014.
[36] Weihai Cortec International Trade Co. Ltd, Plastic Spacer for RO Membrane Rolling, (2015) Shandong, China.
[37] P. Gleick, Basic water requirements for human activities: meeting basic needs. Water International, Water Int. 21 (1996) 83–92.
[38] MATLAB, version 8.6.0 (R2015b), (2010) Natick, Massachusetts.
[39] K. Deb, T. Goel, Controlled elitist non-dominated sorting genetic algorithms for better convergence, Lecture Notes in Computer Science, Springer Berlin Heidelberg, 1993, pp. 67–81.
[40] M. Srinivas, L. Patnaik, Adaptive probabilities of crossover and mutation in genetic algorithms, IEEE Trans. Syst. Man Cybern. 24 (4) (1994) 656–667.
[41] K. Deb, A. Pratap, S. Agarwal, T. Meyarivan, A fast and elitist multiobjective genetic algorithm: NSGA-II, IEEE Trans. Evol. Comput. 6 (2) (2002) 182–197.
[42] R.K. McGovern, S.M. Zubair, J.H. Lienhard V, The cost effectiveness of electrodialysis for diverse salinity applications, Desalination 348 (2014) 57–65.
[43] Y. Kim, W.S. Walker, D.F. Lawler, Electrodialysis with spacers: effects of variation and correlation of boundary layer thickness, Desalination 274 (1–3) (2011) 54–63.
[44] J.-H. Min, H.-S. Kim, Effect of operating conditions on the treatment of brackish groundwater by electrodialysis, Desalin. Water Treat. 51 (January 2015) (2013) 5132–5137.
[45] M.A. Anderson, A.L. Cudero, J. Palma, Capacitive deionization as an electrochemical means of saving energy and delivering clean water. Comparison to present desalination practices: will it compete? Electrochim. Acta 55 (12) (2010) 3845–3856.